Applied Catalysis B: Environmental 129 (2013) 409–415

Contents lists available at SciVerse ScienceDirect

Applied Catalysis B: Environmental

journal homepage: www.elsevier.com/locate/apcatb

Removal of 4-chlorophenol from wastewater: Preparation, characterization and photocatalytic activity of alkaline earth oxide doped TiO_2

Gulin Selda Pozan*, Ayca Kambur

Istanbul University, Faculty of Engineering, Chemical Engineering Department, Avcilar, 34320 Istanbul, Turkey

ARTICLE INFO

Article history:
Received 18 May 2012
Received in revised form
11 September 2012
Accepted 13 September 2012
Available online 8 October 2012

Keywords:
Photocatalysis
4-Chlorophenol
Alkaline earth oxide
TiO_2
UV irradiation
Characterization

ABSTRACT

Alkaline earth oxide (MgO, CaO, SrO) doped TiO_2 catalysts prepared by impregnation method were successfully used in the photocatalytic degradation of 4-chlorophenol (4-CP) under UV irradiation. The materials were characterized by XRD, BET, FT-IR, DRS, PL, SEM and TEM techniques. Alkaline earth metal oxides resulted in an enhanced efficiency of the TiO_2 photocatalyst. The 10 wt% MgO TiO_2 showed the highest percentage of 4-CP degradation (100%) and highest reaction rate (0.82 mg L^{-1} min^{-1}) in 1 h. It was also found that the catalytic activity of 10MgO-TiO_2 was found to be higher than nano TiO_2 and P-25 photocatalyst. The photocatalytic performances are in the orders of: 10MgO/TiO_2 > 10CaO/TiO_2 > 10SrO/TiO_2. Alkaline earth oxide effectively decreases the band gap of the TiO_2. The enhanced adsorption of 4-CP over the catalyst surface and decrease in particle size as a result of Mg^{2+} loading is suggested to be the cause for higher activity of the catalyst. The profound effect of alkaline earth oxide doped TiO_2 for 4-chlorophenol is generally considered due to the entry of Mg^{2+} into the lattice of nano TiO_2 and high dispersion.

1. Introduction

Hazardous water soluble phenolic compounds are continuously introduced in the environment through domestic and industrial activities, representing a severe toxicological risk. 4-Chlorophenol (4-CP), a known endocrine disruptor is toxic and non-biodegradable, present in wastewater as by-products of pulp and paper, dyestuff, pharmaceutical and agrochemical industries [1,2]. Conventional wastewater treatment methods like chemical precipitation, activated carbon adsorption and ion-exchange processes are usually effective in the removal of these compounds in wastewater. However, they transfer the contaminants from one medium to another and hence further treatment or disposal is required. Biodegradation of 4-CP is not only slow and incomplete but also the by-products are more toxic than the contaminants [3–5]. Photocatalysis has been reported as an effective method for treating a wide range of pollutants both from water and air. TiO_2 has emerged as the most viable semiconductor photocatalyst as it is stable in aqueous medium and is tolerant to both acidic and alkaline media [6,7].

Several research groups have reported the reaction mechanisms and the reaction rate equations for the photocatalytic degradation of phenol and different chlorophenols [8–10]. Most of the research groups have used fine powders of semiconductor oxides [11,12] as photocatalysts, e.g. TiO_2, ZnO and WO_3. Others have modified the catalyst surface structure with another metal oxide.

In addition, many studies have been devoted to the improvement of photocatalytic efficiency of TiO_2, such as depositing noble metals [13–16] and doping metal or nonmetal ions [17–20].

Venkatachalam et al. have investigated the physiochemical properties of Zr^{4+} doped nano TiO_2 and correlation of these properties in the photocatalytic activity of TiO_2 for 4-CP degradation. The researchers have found that Zr^{4+} doped nano TiO_2 shows higher photocatalytic activity compared with undoped nano TiO_2 for 4-chlorophenol degradation [21].

Inoue and Khono have shown that the combination of either barium titanate or sodium hexatitanate with ruthenium oxide leads to active photocatalysts for water decomposition [22–24]. These types of catalysts present a UV diffuse reflectance spectra with absorption between 320 and 410 nm [23].

In this paper, alkaline-loaded TiO_2 nanoparticles were prepared by impregnation method and 4-chlorophenol was used as a model pollutant to evaluate the photocatalytic activity of the catalysts under UV irradiation. One of the aims of this study is to investigate the effects of some earth alkaline basic oxides, MgO, CaO and SrO on the structural and surface properties of TiO_2 and second aim is to obtain the information analyzed by various techniques (XRD, DRS, FT-IR, PL, SEM and TEM-EDS), as well to explain the relationship between the structure of the catalysts and photocatalytic activities.

* Corresponding author. Tel.: +90 212 473 70 70x17789.
E-mail address: gpozan@istanbul.edu.tr (G.S. Pozan).

0926-3373/$ – see front matter © 2012 Elsevier B.V. All rights reserved.
http://dx.doi.org/10.1016/j.apcatb.2012.09.050

2. Experimental

2.1. Materials

Starting materials for catalyst preparation were $Mg(NO_3)_2{\cdot}6H_2O$, $Ca(NO_3)_2{\cdot}4H_2O$, $Sr(NO_3)_2$ (reagent grade, Aldrich) and Degussa P25 (consisting of 75% anatase and 25% rutile with a specific BET-surface area of 50 $m^2\,g^{-1}$ and primary particle size of 20 nm). The organic compounds used in the photocatalytic experiments were phenol and 4-chlorophenol (99.9% purity, Aldrich). All the solutions were prepared with deionized water. Mobile phase for HPLC analysis was prepared with methanol (HPLC grade, Fluka Company).

2.2. Catalyst preparation

TiO_2 nano-powders were prepared titanium tetrachloride and deionized water as the starting materials [25].

Alkaline metal solutions were prepared by dissolving $Mg(NO_3)_2{\cdot}6H_2O$, $Ca(NO_3)_2{\cdot}4H_2O$, $Sr(NO3)_2$ in distilled water. Alkaline earth oxide doped TiO_2 catalysts were prepared by incipient wetness impregnation from aqueous metal solutions. The impregnated TiO_2 was dried at 105 °C for 16 h, and it was calcined in air at 500 °C for 3 h. The resultant alkaline earth oxide loaded $TiO_2$was ground at a constant vibration rate of 300 rpm for 15 min in a Retsch MM 200 vibrant-ball mill by 12 mm ZrO_2 milling ball in ZrO_2 milling container. Alkaline earth oxide loading of the catalyst was nominally 5, 10 and 15 wt% and reported as the weight percentages of their common oxides. For instance, $5MgO/TiO_2$ means that the catalyst contained nominally 5MgO by weight and deposited on to TiO_2 support.

2.3. Catalyst characterization

The composition of the catalyst was determined using Thermo Elemental X Series ICP-MS.

The BET surface areas of the samples were determined by nitrogen adsorption–desorption isotherm measurement at 77 K. The samples were degassed at 200 °C prior to the actual measurements.

Powder X-ray diffractions of samples were obtained using a Rigaku D/Max-2200 diffractometer with the Cu Kα (λ = 1.540) radiation. Samples were scanned from 10 to 80 at a rate of 2°/min (in 2Θ). The sizes of the crystalline domains were calculated by using the Scherrer equation, $t = C\lambda/B\cos\Theta$, where λ is the X-ray wavelength (Å), B is the full width at half maximum, Θ is Bragg angle, C is a factor depending on crystallite shape (taken to be one), and t is the crystallite size (Å).

The morphology and size distribution of the photocatalysts were recorded by scanning electron microscopy (JEOL/JSM-6335F) and transmission electron microscopy (JEOL HRTEM 2100).

Fourier transform infrared spectra were recorded on a Perkin Elmer Precisely Spectrum One spectrometer at ambient conditions by using KBr as diluent. All measurements were at 4 cm^{-1} resolution and 100 scans.

Photoluminescence measurement (PL) was carried out on a fluorescence spectrophotometer (Agilent Technologies-Cary Eclipse) using a Xenon lamp as the excitation source at room temperature. The sample was dispersed in ethanol using ultrasonic bath and the excitation wavelength used in PL measurement was 325 nm.

2.4. Evaluation of photocatalytic activity

The photoactivity studies were carried out at atmospheric pressure and room temperature (298 K). In a typical experiment, 100 mg catalyst was dispersed in 50 mL 4-chlorophenol solution of initial concentration 25 mg L^{-1} and neutral pH (pH 5.2) under magnetic stirring.

4-Chlorophenol photooxidation runs were done with quartz batch-photoreactor of cylindrical shape. LUZCHEM LZC-5 photoreactor system was used in all experiments. The light source used was 16 W UV-B lamp (LUZCHEM LZC-UVB). The spectral irradiance of the UV lamp is from 303 to 578 nm and the illumination distance is 18 cm from the target. The light intensity of UV lamp used for degradation experiments was recorded with an UV/visible powermeter (Smart Sensor- AR823). The photoreactor system had a magnetic stirrer and it was used to achieve uniform conditions in the reacting mixture. Before the UV light was turned on, the solution was stirred for 60 min to ensure good adsorption equilibrium between the catalyst and the solution. After irradiation for 1 h, the phenol solution was filtered through a membrane filter (pore size 0.45 mm) and the filtrate was used for TOC measurement with a TOC-V, Shimadzu equipment. The concentration of phenol and products were analyzed by HPLC equipped with C-18 column. The mobile phase used in HPLC was a mixed solvent of methanol and water (70/30, v/v) with a flow rate of 1 ml/min.

3. Results and discussion

3.1. Catalyst characterization

The actual weight percentages of the catalysts were obtained by ICP- MS analysis and are reported in Table 1. The calculated wt% of the catalysts and the ICP values were almost similar.

BET surface areas of supported metal oxide catalysts were measured, and listed in Table 1, $10SrO/TiO_2$ (9 $m^2\,g^{-1}$) < $10CaO/TiO_2$ (12 $m^2\,g^{-1}$) < $10MgO/TiO_2$ (22 $m^2\,g^{-1}$).

TiO_2 has a surface area of 40 $m^2\,g^{-1}$. As an example, after impregnation, BET surface area of $10MgO/TiO_2$ has decreased down to 22 $m^2\,g^{-1}$. For the MgO-TiO_2 series, surface areas decreased with an increase in the amount of MgO. This effect may be attributed to the presence of metallic oxides in the poremouths of the TiO_2 pores and channels.

The crystallite sizes of the catalysts are calculated according to the Scherrer Formula and the results are listed in Table 1.

Table 1
Metal oxide content, crystallite size, specific surface area, band gap, reaction rate constant and photocatalytic degradation efficiency over 1 h (%).

Catalyst	Metal oxide content (wt%)	Crystallite size (nm)	Specific surface area ($m^2\,g^{-1}$)	Band gap (eV)	k_r[a]	4-Chlorophenol degradation efficiencies over 1 h (%)
TiO_2 (P25)		32	50	3.12	0.01	7
TiO_2 (synthezied)		43	40	3.02	0.71	91
$5MgO/TiO_2$	4.85	27	28	2.83	0.64	95
$10MgO/TiO_2$	9.50	34	22	2.85	0.82	100
$15MgO/TiO_2$	14.90	39	16	2.87	0.79	87
$10CaO/TiO_2$	9.38	46	12	2.92	0.47	75
$10SrO/TiO_2$	9.40	55	9	2.88	0.34	68

[a] Reaction rate constant (mg L^{-1} min^{-1}).

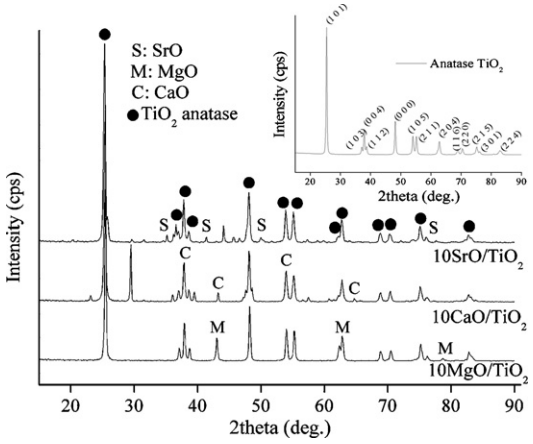

Fig. 1. XRD patterns for 10MgO-TiO_2, 10CaO-TiO_2 and 10SrO-TiO_2 catalysts. Inset shows the XRD pattern of TiO_2 (synthesized).

The diffraction patterns of various metal oxides impregnated TiO_2 catalysts were obtained. The XRD patterns of the catalysts are shown in Fig. 1. Anatase TiO_2 was the major crystalline phase detected on the X-ray diffraction pattern. Peaks appearing at 2θ: 25.4, 37.0 37.9, 38.6, 47.9, 54.0, 55.2, 62.9, 68.9, 70.4, 75.2, 76.2, 83.1 correspond to the diffraction patterns of (1 0 1), (1 0 3), (0 0 4), (1 1 2), (0 0 0), (1 0 5), (2 1 1), (2 0 4), (1 1 6), (2 2 0), (2 1 5), (3 0 1) and (2 2 4), respectively, of the pure anatase phase of TiO_2. In XRD patterns, the diffraction pattern of tetragonal MgO (JCPDS 45-0946), cubic CaO (JCPDS 82-1691), and tetragonal SrO (JCPDS 48-1477) were detected. TiO_2 crystallite size increased as manganese oxide content increased.

The morphology and particle size of 10MgO/TiO_2, 10CaO/TiO_2 and 10SrO/TiO_2 oxide calcined at 500 °C were observed by TEM in Fig. 2a, b and c, respectively. TEM pictures confirmed that the alkaline metal doped nano TiO_2 particles are spherical in shape with an average grain size of 45–65 nm. 10MgO/TiO_2 catalyst has uniform morphology with the particle size of 30–50 nm, whereas, 10CaO/TiO_2 and 10SrO/TiO_2 are in irregular sizes and shapes and also the particle size of 10CaO/TiO_2 and 10SrO/TiO_2 are around 15–50 nm, 15–70 nm, respectively. These results are in good agreement with XRD data. TEM pictures and (Energy Dispersive Spectroscopy) EDS analyzes of catalysts gave convincing evidence for the presence of alkaline oxide on the surface nano TiO_2. MgO dispersion was observed on the whole surface of nano TiO_2 in comparison to CaO and SrO. The observed dispersion for alkaline oxide on the surface nano TiO_2 follows the order 10MgO/TiO_2 > 10CaO/TiO_2 > 10SrO/TiO_2. MgO showed high dispersion on nano TiO_2 than CaO and SrO. It has high photocatalytic activity because of the homogenously high dispersion on nanoTiO_2. This study clearly established the role of Mg^{2+} in decreasing the size of nano TiO_2. The profound effect of 10MgO/TiO_2 catalyst for 4-chlorophenol degradation is generally considered due to the small particle size and and high dispersion of MgO content than that of the pure nanoTiO_2 photocatalyst.

The impact of alkaline earth oxide doping on the band gap of TiO_2 was investigated using UV–vis diffuse reflectance spectroscopy and the results are shown in Fig. 3. Corresponding calculated band gap values are also reported in Table 1. The calculated band gap of pure TiO_2 is 3.02 eV, whereas the band gap is lowered to 2.85 eV by the addition of 10 wt % MgO. In addition, the lowest crystallite size (particle size) (33 nm) and the lowest band gap energy (2.85 eV) were obtained with the 10MgO/TiO_2 binary oxide catalyst varied with different alkaline oxide.

Photocatalyst samples were also analyzed by FTIR spectroscopy. FTIR spectra of pure and alkaline metal doped TiO_2 showed

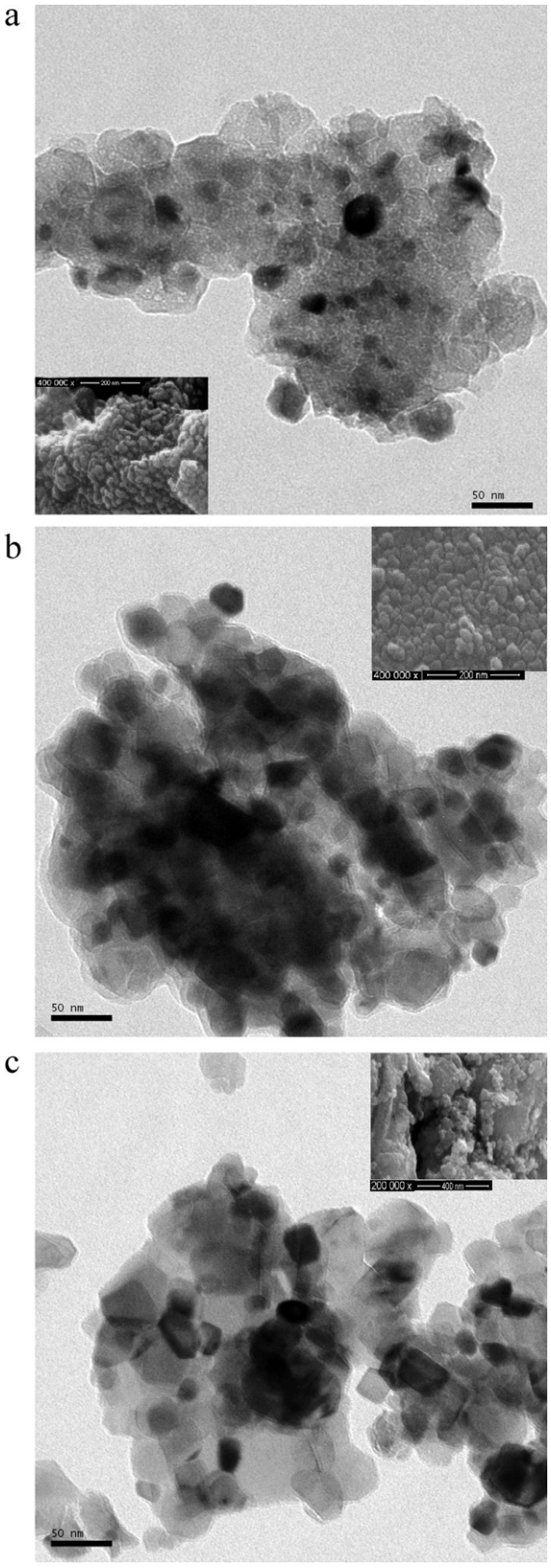

Fig. 2. (a) TEM pattern of 10MgO-TiO_2 (inset shows SEM micrograph of 10MgO-TiO_2). (b) TEM pattern of 10CaO-TiO_2 (inset shows SEM micrograph of 10CaO-TiO_2). (c) TEM pattern of 10SrO-TiO_2 (inset shows SEM micrograph of 10SrO-TiO_2).

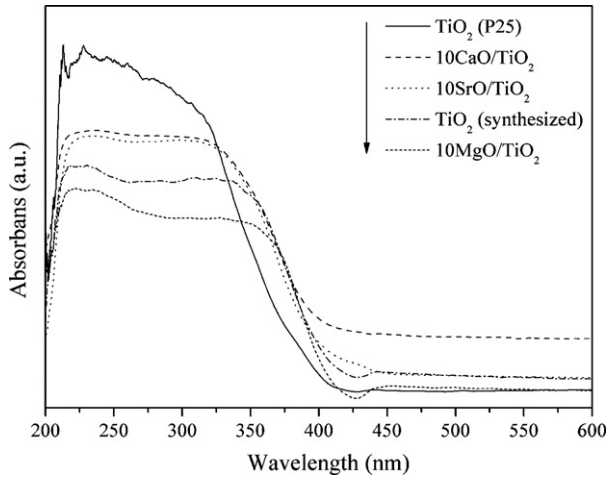

Fig. 3. FTIR spectra of TiO_2 and alkaline earth oxide doped TiO_2.

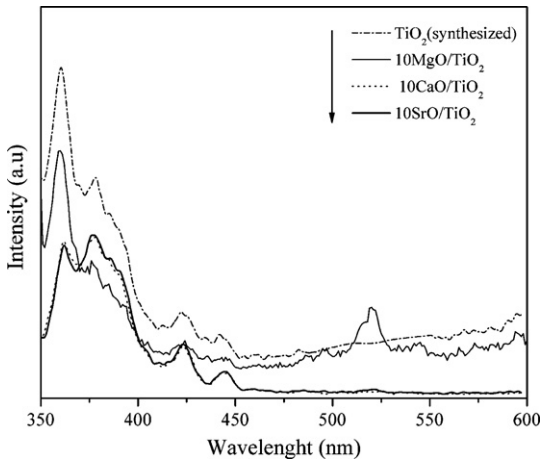

Fig. 5. The fluorescence emission spectra of alkaline metal oxide doped (MgO, CaO, SrO) nano TiO_2 catalysts.

peaks corresponding to stretching vibrations of O—H and bending vibrations of adsorbed water molecules around 3350–3450 and 1620–1635 cm^{-1}, respectively. The intensity of these peaks became less with increase in calcination temperature, indicating the removal of large portion of adsorbed water from TiO_2. The broad intense band below 1200 cm^{-1} is due to Ti—O—Ti vibration (Fig. 4). This peak appears quite unsymmetrical whereas the same for 10 wt% MgO doped nano TiO_2 appears symmetrical. There is significant shift in the peak maximum to high energies in the FT-IR spectrum of Mg^{2+} doped nano TiO_2 compared to parent nano TiO_2. Since the atomic mass of magnesium is lower than titanium, one could expect shifting of Ti—O—Mg vibration to higher energy than Ti—O—Ti vibration. In addition, the new peak appeared at 1091 cm^{-1} for $10MgO/TiO_2$ is also taken into consideration for isomorphic substitution. This peak is tentatively assigned to framework Ti—O—Mg vibration. This additional peak was not observed in 10 wt% CaO and 10 wt% SrO doped nano TiO_2. Hence FT-IR spectral study established clearly the entry of Mg^{2+} and not Ca^{2+} and Sr^{2+} into the lattice of nano TiO_2. FTIR spectra of $10CaO/TiO_2$ revealed the presence of two peaks at 877 and 716 cm^{-1} which are the characteristic bands of Ca—O [26].

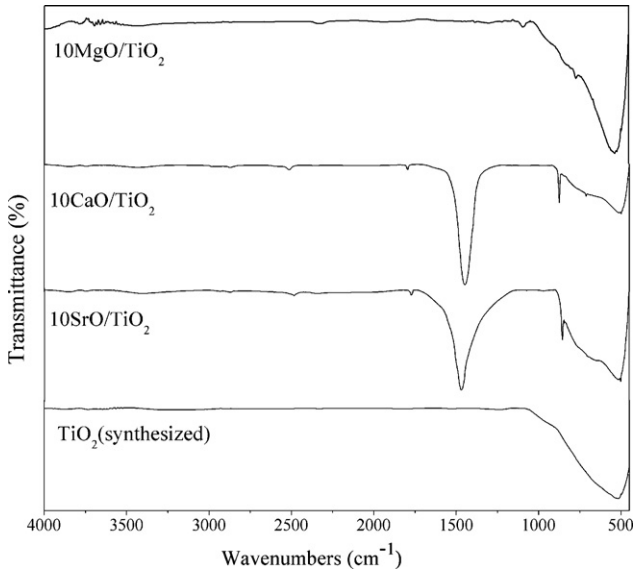

Fig. 4. UV–vis diffuse reflectance spectra of catalysts.

Furthermore, the bands observed at about 1450 and 1780 cm^{-1} indicate the presence of Ti—O bands for $10CaO/TiO_2$ and $10SrO/TiO_2$ [27].

The entry of Mg^{2+} into the lattice of nano TiO_2 creates charge compensating anion vacancy, which may enhance the adsorption of 4-CP [28]. Further, the dopant ion Mg^{2+} with ionic radius (0.86 Å), larger than Ti^{4+} (0.75 Å) but smaller than O^{2-} (1.31 Å), can either isomorphously substituted or interstitially introduced into the matrix of nano TiO_2 to produce oxygen vacancies which accelerate the transition and nanocrystalline growth of anatase nano TiO_2 [29]. The formation of Ti—O—Mg inhibits the transition of TiO_2 phase and prevents the agglomeration of TiO_2 nano particles. Hence, the entry of Mg^{2+} ions into the TiO_2 lattices suppressed the particle growth and consequently increased the band gap value of nano TiO_2, which minimized the electron–hole recombination during the photocatalytic degradation organic compounds [30]. The framework substitution of Mg^{2+} in TiO_2 lattice is also confirmed from the FT-IR spectrum of catalyst. In the case of Ca^{2+} and Sr^{2+} doped nano TiO_2, no evidence for the isomorphic substitution of Ca^{2+} and Sr^{2+} were observed since the ionic radius of Ca^{2+} (1.08) and Sr^{2+}(1.21) are higher than Ti^{4+} [31].

The fluorescence emission spectra of alkaline metal oxide doped (MgO, CaO, SrO) nano TiO_2 catalysts are presented in Fig. 5. The emission spectra of MgO doped nano TiO_2 give convincing evidence for the oxygen vacancy in nano TiO_2. Since the excitation was carried out under equal adsorption conditions at 325 nm, decrease in emission intensity was observed with MgO doped nano TiO_2 catalyst compared to pure nano TiO_2. The decrease in the emission intensity may also due to introduction of new defect sites such as oxide ion vacancy [32]. Besides, the as-synthesized $10MgO/TiO_2$ nanoparticles demonstrated a remarkable and broad visible light emission centered at about 520 nm compared to $10CaO/TiO_2$ and $10SrO/TiO_2$ catalysts.

CaO and SrO doped nano TiO_2 also exhibited less intensity of emission than pure nano TiO_2. Moreover, it can be clearly seen that the emission spectra of both $10CaO/TiO_2$ and $10SrO/TiO_2$ catalysts are quite similar. This low intensity emission is ascribed to low absorption of light by CaO and SrO doped nano TiO_2 due to the formation of large CaO and SrO particles on its surface. In other words, the presence of large CaO and SrO particles in the poremouths of the TiO_2 pores and channels may block significantly the entry of UV light into TiO_2 particles to excite electrons. These results are in good agreement with activity results.

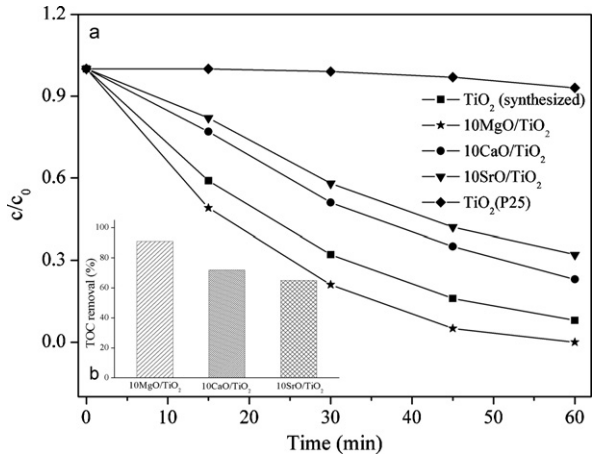

Fig. 6. Time course of the adsorption of 4-chlorophenol by TiO_2 (synthesized), TiO_2 (P25) and alkaline earth oxide doped TiO_2 under UV irradiation. Inset shows the impact of alkaline earth oxide on TOC removal in the 4-chlorophenol degradation.

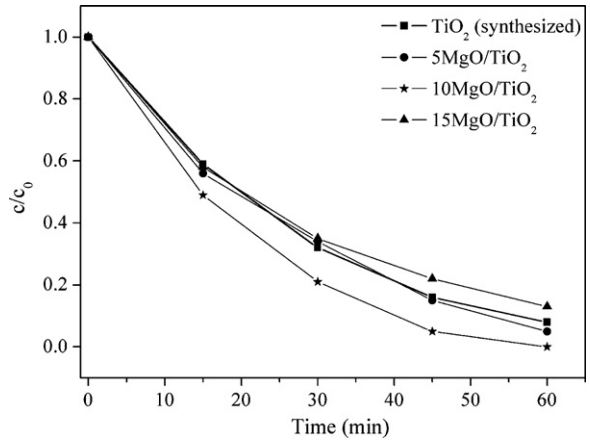

Fig. 7. Effect of various MgO loading on 4-chlorophenol photodegradation at 25 °C.

3.2. Evaluation of photocatalytic activity

In general, the diffusion rate of adsorbed reactive species on the surface is faster than the photocatalytic reaction rate. Therefore, the photocatalytic reaction is the rate control step. The photocatalytic degradation can be described with the Langmuir–Hinshelwood equation [33]:

$$\frac{1}{r_0} = \frac{1}{k_r K_{ads} c_0} + \frac{1}{k_r}$$

r_0 is the initial reaction rate ($mg\,L^{-1}\,min^{-1}$), k_r the Langmuir–Hinshelwood reaction rate constant ($mg\,L^{-1}\,min^{-1}$) and K the Langmuir adsorption constant ($L\,mg^{-1}$).

The photocatalytic degradation performance for TiO_2, P25 and alkaline oxide-TiO_2 binary oxide catalyst were monitored for the oxidative degradation of 4-chlorophenol and the results are shown in Fig. 6a.

Fig. 6b presents the TOC removal results on the photocatalytic degradation of 4-chlorophenol with MgO/TiO_2, CaO/TiO_2 and SrO/TiO_2. 25 ppm 4-chlorophenol can be completely degraded in 60 min by $10MgO/TiO_2$ sample at an initial pH of 5 and 91% TOC removal can be achieved in 60 min. This result emphasizes the achievement of the total mineralization.

The photocatalytic degradation performances for these catalysts were monitored for the oxidative degradation of 4-chlorophenol and the results are shown in Table 1. 91% degradation of phenol was achieved with the pure nano TiO_2 catalysts under UV light irradiation for 60 min. The performance of MgO/TiO_2 catalysts with varying MgO loadings was also studied (Fig. 7). The degradation ability for the MgO/TiO_2 catalyst increased with an increase in the amount of MgO loadings to TiO_2. The 10 wt% MgO showed the highest percentage of phenol degradation (100%), however, after that weight percentage, there was noticeable change in the reactivity and the value remained the same with further loadings of TiO_2 (Table 1). Also, 4-chlorophenol degradation decreases from 100 to 87% with the 15 wt% MgO mixed with TiO_2. In fact, a decrease in activity could probably be explained by partial blocking of the active species of TiO_2 due to the formation of larger MgO particles at higher MgO loadings. The results showed that surface area and particle size of samples were changed with the loading of MgO. Addition to this result, tendency of MgO to form larger particles on TiO_2 surface has also caused to lower the conversion of 4-chlorophenol.

In addition, the catalytic activity of 10 wt% MgO to TiO_2 and nano TiO_2 prepared were found to be higher than P-25. Although the decrease in surface area of $10MgO/TiO_2$ catalyst and nano TiO_2 prepared were comparable even lower than TiO_2 P-25, they showed high activity. However, the changes in surface areas were not as drastic as the changes in catalytic activities, hence, the activity comparisons were due to the active species on the surface.

Xu and Langford investigated the photocatalytic activity of titanium oxide supported on ZSM5, zeolite A, silica, and alumina using the photooxidation of 4-chlorophenol and acetophenone. It was found that the photocatalytic activity of TiO_2/ZSM5 was higher than TiO_2 powder prepared and Degussa P25 [34].

The photocatalytic activity was affected by the acid–base properties of the catalyst. In general, basicity of alkaline earth oxide increases from MgO to BaO. It is clearly seen that the activity varies in parallel with the basicity of alkaline earth oxide. Consequently, the addition of strong basic alkaline oxide induced a decrease in both the photocatalytic activity and the final conversion (after 1 h of reaction time) in oxidative degradation of 4-chlorophenol over catalysts.

Leyva et al. prepared several barium-lithium titanates and tested photocatalytic activity for the degradation of phenol and 4-CP. The results of the photocatalytic degradation of 4-CP showed that the conversion of 4-CP was obtained 21.3% after 24 h of reaction [35].

HPLC analysis performed during the photocatalytic degradation of 4-chlorophenol. Hydroquinone (HQ; 4-hydroxyphenol), Catechol (CT; 2-hydroxyphenol), phenol (Ph), hydroxyhydroquione (HHQ) and 2-chlorophenol (2-CP) were detected as intermediates. And also ring-opening products are supposed to be short chain acids, such as, acetic acid, maleic acid, oxalic acid, etc. [36], they were identified by GC–MS analysis.

The degradation profile for 4-chlorophenol is shown in Fig. 8a–c along with the evolution profile of intermediates. Besides, the distributions of intermediates also were compared in different alkaline oxide-TiO_2 catalysts.

Three major intermediates, HHQ, CT and 2-CP, were detected during the degradation of 4-chlorophenol for $10MgO/TiO_2$. In addition to these products, Ph and HQ were also detected in very low concentration.

Unlike $10MgO/TiO_2$, CT was detected as main intermediate by using $10CaO/TiO_2$. According to HPLC results, the concentration of catechol consistently increased in reaction time. However, in addition to CT, three intermediates, namely HQ and Ph were detected in very low concentration.

Similar to the $10CaO/TiO_2$ binary oxide catalyst, CT was detected as main intermediate by using $10SrO/TiO_2$. However, during the degradation of 4-chlorophenol, in addition to CT, three intermediates, namely HQ and Ph, were detected in very low concentration.

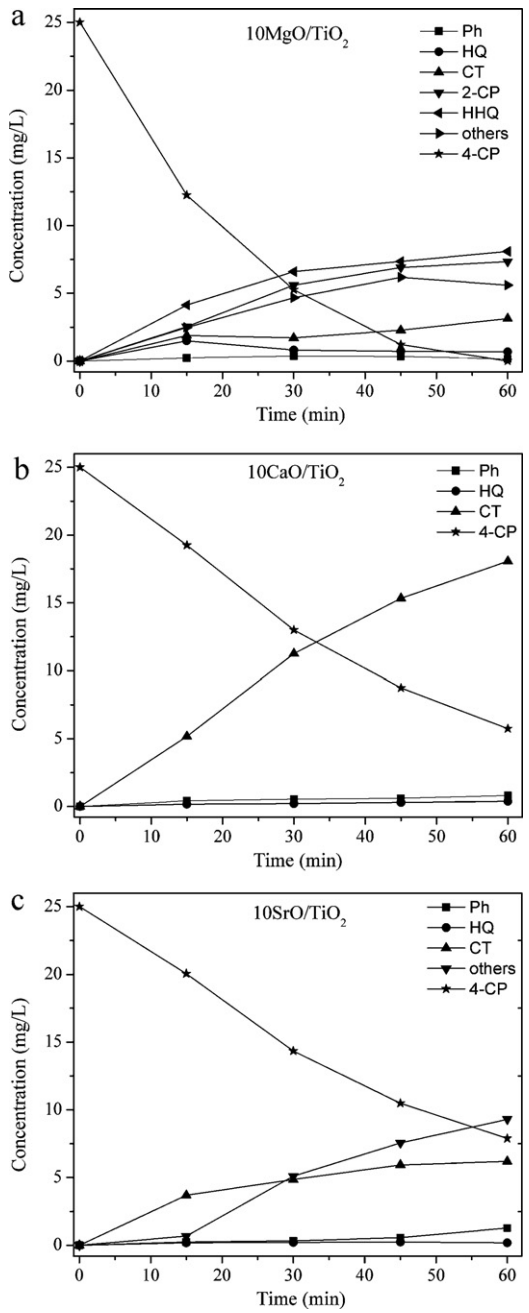

Fig. 8. Concentration profiles for intermediates obtained during the photocatalytic oxidation reaction using (a) 10MgO-TiO_2, (b) 10CaO-TiO_2, (c) 10SrO-TiO_2.

2-Chlorophenol was not observed for 10CaO/TiO_2 and 10SrO/TiO_2 loading during the photocatalytic oxidation reaction.

However, when the 4-chlorophenol was degraded by synthesized TiO_2, the concentration of the intermediates (HQ, CT, 2-CP and Ph) were lower than the concentration of alkaline metal oxide doped TiO_2 catalysts. Moreover, ring-opening products were found in higher concentration by using TiO_2 compared to alkaline metal oxide doped TiO_2 catalysts.

Besides, ring-opening products were only observed by using 10MgO/TiO_2 and 10SrO/TiO_2. These intermediates undergo further photocatalytic oxidation to ring cleavage to yield carboxylic acids and aldehydes, which give CO_2 and H_2O due to decarboxylation.

It can be seen that 2-CP and HHQ were only obtained was for 10MgO/TiO_2 loading. These results indicate that 10CaO/TiO_2 and 10SrO/TiO_2 catalysts can be slightly activated by UV light.

It is noteworthy to mention that, catechol were detected higher concentration compared to BQ and HQ by using 10MgO/TiO_2, 10CaO/TiO_2 and 10SrO/TiO_2. However, CT is likely to be more advantageous for the complete mineralization of phenol than conversion to BQ or HQ, as reported by Santos et al. [37], because CT is decomposed to oxalic acid, and then to CO_2 and water, whereas the pathways of mineralization of BQ and HQ are much longer.

It should be noted that, some structural features of catalyst play a significant role during the photocatalysis. These results confirm that 10MgO/TiO_2 is more active than the other catalysts. These results may also indicate that the photochemical reaction plays an important role for the degradation of 4-chlorophenol under these conditions.

4. Conclusions

Alkaline earth oxide doped TiO_2 catalysts prepared by impregnation method were successfully used in the photocatalytic degradation of 4-CP under UV irradiation. This doped nano TiO_2 exhibits enhanced photocatalytic activity in the degradation of 4-CP. Alkaline earth oxide effectively decreases the band gap of the TiO_2. The 10 wt% MgO TiO_2 showed the highest percentage of 4-CP degradation (100%) and highest reaction rate (0.82 mg L^{-1} min^{-1}) in 1 h. Also, the catalytic activity of 10MgO-TiO_2 was found to be higher than nano TiO_2 and P-25 photocatalyst. The entry of Mg^{2+} into the lattice of nano TiO_2 is evidenced by XRD and FT-IR studies. Ca^{2+} and Sr^{2+} are not observed to take the lattice position of nano TiO_2 due to its large ionic radius.

According to TEM-EDS analysis, CaO and SrO showed lower dispersion on nano TiO_2 than MgO. The enhanced adsorption of 4-CP over the catalyst surface and decrease in particle size as a result of Mg^{2+} loading is suggested to be the cause for higher activity of the catalyst.

Acknowledgement

This work was supported by the Research Fund of the Istanbul University.

References

[1] L.H. Keith, Pure and Applied Chemistry 70 (1998) 2319–2326.
[2] J. Theurich, M. Lindner, D.W. Bahnemann, Langmuir 12 (1996) 6368–6376.
[3] A.K. Jain, V.K. Gupta, S. Jain, Suhas, Environmental Science and Technology 38 (2004) 1195–1200.
[4] D. Chen, A.K. Ray, Applied Catalysis B: Environmental 23 (1999) 143–157.
[5] K.B. Sherrard, P.J. Marriott, R.G. Amiet, M.J. McCormick Ray, C.K. Millington, Chemosphere 33 (1996) 1921–1940.
[6] M.A. Fox, M.T. Dulay, Chemical Reviews 93 (1993) 341–357.
[7] S. Anandan, A. Vinu, N. Venkatachalam, B. Arabindoo, V. Murugesan, Journal of Molecular Catalysis A: Chemical 256 (2006) 312–320.
[8] P. Pichat, C. Mallard, C. Guillard, H. Courbon, Environmental Science and Technology 28 (12) (1994) 2176–2183.
[9] J.R. Bolton, L. Sun, Journal of Physical Chemistry 100 (1996) 4127–4134.
[10] K. Hasegawa, S. Takeuchi, Environmental Science and Technology 27 (9) (1993) 1819–1825.
[11] J.M. Herrmann, P. Pichat, Journal of the Chemical Society, Faraday Transactions 1 (76) (1980) 1138–1146.
[12] M.A. Fox, Chemtech (1992) 680–685.
[13] M. Bowker, D. James, P. Stone, R. Bennett, N. Perkins, L. Millard, J. Greaves, A. Dickinson, Journal of Catalysis 217 (2003) 427–433.
[14] H. Einaga, T. Ibusuki, S. Futamura, Environmental Science and Technology 38 (2004) 285–289.
[15] Y.X. Li, G. Lu, S. Li, Journal of Photochemistry and Photobiology A 152 (2002) 219–228.
[16] T.G. Schaaff, D.A. Blom, Nano Letters 2 (2002) 507–511.
[17] M. Mrowetz, W. Balcerski, A.J. Colussi, M.R. Hoffmann, Journal of Physical Chemistry B 108 (2004) 17269–17273.
[18] J. Premkumar, Chemistry of Materials 16 (2004) 3980–3981.
[19] S. Jeon, P.V. Braun, Chemistry of Materials 15 (2003) 1256–1263.
[20] A. Patra, C.S. Friend, R. Kapoor, P.N. Prasad, Chemistry of Materials 15 (2003) 3650–3655.

[21] N. Venkatachalam, M. Palanichamy, B. Arabindoo, V. Murugesan, Journal of Molecular Catalysis A: Chemical 266 (2007) 158–165.
[22] Y. Inoue, Y. Asai, K. Sato, Journal of the Chemical Society, Faraday Transactions 90 (5) (1994) 797–802.
[23] Y. Inoue, M. Khono, K. Ogura, K. Sato, Studies in Surface Science 101(A) (1996) 143–152.
[24] Y. Inoue, T. Kubokawa, K. Sato, Journal of Physical Chemistry 95 (10) (1991) 4059–4063.
[25] A. Kambur, G.S. Pozan, I. Boz, Applied Catalysis B: Environmental 115–116 (2012) 149–158.
[26] Academic Press Inc., New York, 1997.
[27] M.F. Morks, Materials Letters 64 (18) (2010) 1968–1971.
[28] K. Nagaveni, M.S. Hegde, G. Madras, Journal of Physical Chemistry B 108 (2004) 20204–20212.
[29] N.I. Al-Salim, S.A. Bagshaw, A. Bittar, T. Kemmitt, M.A. James, A.M. Mills, M.J. Ryan, Journal of Materials Chemistry 10 (2000) 2358–2363.
[30] M.S.P. Francisco, V.R. Mastelaro, Chemistry of Materials 14 (2002) 2514–2518.
[31] Pauling, L., Cornell University Press, New York, 1960.
[32] K. Nagaveni, M.S. Hegde, G. Madras, G. Madras, Journal of Physical Chemistry B 108 (2004) 20204–20212.
[33] Y. Xu, C.H. Langford, Journal of Photochemistry and Photobiology A 133 (2000) 67–71.
[34] Y. Xu, C.H. Langford, Journal of Physical Chemistry 99 (1995) 11501–11507.
[35] E. Leyva, E. Moctezuma, M.G. Ruíz, L. Torres-Martínez, Catalysis Today 40 (1998) 367–376.
[36] B. Tryba, A.W. Morawski, M. Inagaki, M. Toyoda, Applied Catalysis B: Environmental 63 (2006) 215–221.
[37] A. Santos, P. Yustos, A. Quintanilla, S. Rodriguez, F. Garcia-Ochoa, Applied Catalysis B: Environmental 39 (2002) 97–113.